Front. Optoelectron. 2016, 9(3): 377–389
DOI 10.1007/s12200-016-0554-y

TUTORIAL ARTICLE

Linear optical signal processing with optical filters: a tutorial

Xinliang ZHANG (✉), Zhao WU

Wuhan National Laboratory for Optoelectronics (WNLO), School of Optical and Electronic Information, Huazhong University of Science and Technology, Wuhan 430074, China

Abstract An effective theoretical analysis method is presented to analyze different linear optical signal processing functions with optical filters reported in literatures. For different applications, the optical filters are supposed to operate on the analog or digital part of the signal separately, namely analog spectrum conversion and digital spectrum conversion. For instance, the return-to-zero (RZ) to non-return-to-zero (NRZ) format conversion for intensity or phase modulated signals are based on the analog spectrum conversion process, while the (N)RZ to (N)RZ phase-shift-keying (PSK) format conversion, logic NOT gate and clock recovery for RZ signals are based on the digital spectrum conversion process. Theoretical analyses with the help of numerical simulation are used to verify the reported experimental results, and all the experimental results can be effectively analyzed with this analytical model. The effect of the transmission spectrum of the filter on the performance of the converted signal is investigated. The most important factor is that the theoretical analysis provides an effective way to optimize the optical filter for different optical signal processing functions.

Keywords linear optical signal processing, format conversion, optical filter, clock recovery, logic gate

1 Introduction

All-optical signal processing can increase the operation speed and decrease the power consumption greatly by processing the signal in optical domain directly and avoiding optical to electrical and electrical to optical conversion process. In recent two decades, all-optical signal processing has been receiving increasingly attention, and many functions have been demonstrated, such as wavelength conversion, format conversion, logic operation, 2R regeneration, clock recovery, and so on. According to operation mechanisms, these optical signal processing functions can be divided into two different kinds: nonlinear signal processing and linear signal processing. For nonlinear kind, optical signal processing functions should be realized with different nonlinear effects in some special media, such as chalcogenide waveguide [1,2], periodically poled lithium niobate (PPLN) waveguide [3], semiconductor optical amplifier (SOA) [4–6], high nonlinear fiber (HNLF) [7,8], and other devices [9,10]. Usually, there exists tradeoff between the conversion efficiency and the operational speed in these nonlinear optical signal processing functions. For linear kind, optical signal processing functions could be easily realized with filtering effect. Based on different filtering devices, some signal processing functions, such as format conversion [11,12], logic gate [13], clock recovery [14], optical differentiation [15] and integration [16,17], and Hibert transformer [18,19], were demonstrated. Because of linear effect, these functions can be demonstrated with extremely simple configuration, no additional noise, no pattern effect and no speed limitation.

In our research group [20–36], delay interferometers (DIs) and microring resonators (MRRs) were mainly exploited to realize various kinds of format conversion functions and clock recovery function. Format conversion functions from return-to-zero (RZ) to non-return-to-zero (NRZ) for on-off-keying (OOK), differential-phase-shift-keying (DPSK) and 4 × 50 Gb/s multichannel RZ-to-NRZ conversion [27], polarization division multiplexed (PDM) format conversion [34,35] demonstrated its flexibility and potential for application in high capacity optical networks. On the other hand, clock recovery function was also analyzed [28] and experimentally demonstrated [36] with MRR. Although many experimental results for linear signal processing have been reported [13,14,20–36], there is no thorough theoretical model to analyze all the experimental results. The most important factor is, there is different requirements of the filtering spectrum for

Received September 24, 2015; accepted January 16, 2016

E-mail: xlzhang@mail.hust.edu.cn

different signal processing functions. One completed theoretical model should be developed to optimize the transfer spectrum of the filter.

In this paper, we tend to present a completed theoretical method to analyze these reported experimental results for linear signal processing. To facilitate the analysis, we decomposed the optical signal into the analog and digital parts, which represent the pulse shape of each symbol and the data information of the symbol sequence, respectively. Then, the optical filter is supposed to operate on the analog or digital spectrum independently for different applications, corresponding to analog spectrum conversion and digital spectrum conversion process, respectively. Based on this model, the operational principle of RZ to NRZ format conversion for intensity and phase modulated signals, (N)RZ to (N)RZ-PSK format conversion, all-optical NOT gate, and clock recovery for RZ signals can all be illustrated. Results show that the RZ-to-NRZ format conversion is based on the analog spectrum conversion process. In this case, the pulse shape of each symbol is changed from RZ to NRZ, while the symbol sequence of the data information remains unchanged. On the other hand, the format conversion from (N)RZ to (N)RZ-PSK, all-optical NOT gate and clock recovery for RZ signals are based on the digital spectrum conversion process. In this case, the data information is changed, while the pulse shape of each symbol remains unchanged.

The rest of this paper is organized as follows. Section 2 describes the principle of spectrum decomposition for the modulated signal and analyzes the characteristics of the analog and digital spectra. Section 3 theoretically demonstrates the operational principle for the signal conversion process, consisting of analog spectrum conversion and digital spectrum conversion process. Section 4 discusses the applicability of the theoretical model and the effect of defective filter on the converted signal, and Section 5 concludes this paper.

2 Spectrum decomposition

2.1 Signal decomposition

Although we could find similar analysis for electrical signal processing in the textbooks, we would like to present the analytical process of spectrum decomposition for the integrity of the theoretical model. Actually, there is also no similar analysis for optical signal processing. Considering a modulated signal, the complex envelop of the electric field is expressed as

$$E(t) = \sum_{k=-\infty}^{+\infty} x_k g(t-kT_s), \tag{1}$$

where $g(t)$ is the pulse shape centered at $t = 0$ which can be NRZ, or RZ with different duty cycles, T_s is the symbol period, and x_k are information symbols that are independent identically distributed (i.i.d.) random variables. $x_k \in \{0, 1\}$, $\{1, -1\}$ and $\{1, j, -1, -j\}$ denote the information symbols of OOK, PSK, and QPSK signals, respectively.

The expression of the electric field can be modified as

$$E(t) = g(t) * \sum_{k=-\infty}^{+\infty} x_k \delta(t-kT_s), \tag{2}$$

where * denotes convolution operation and δ represents the Dirac function. $g(t)$ is the analog part of the signal, which represents the pulse shape of each symbol. While $\sum_{k=-\infty}^{+\infty} x_k \delta(t-kT_s)$ is the digital part of the signal, which represents the data information of the signal.

The spectrum of the modulated signal is the Fourier transformation of its electric field and expressed as

$$F(f) = G(f) \cdot X(f), \tag{3}$$

where $G(f)$ and $X(f)$ are the analog and digital spectra of the signal, which are the Fourier transformation of $g(t)$ and $\sum_{k=-\infty}^{+\infty} x_k \delta(t-kT_s)$, respectively, and are obtained by

$$G(f) = \int_{-\infty}^{+\infty} g(t) \exp(-j2\pi ft) dt, \tag{4}$$

$$X(f) = \int_{-\infty}^{+\infty} \sum_{k=-\infty}^{+\infty} x_k \delta(t-kT_s) \exp(-j2\pi ft) dt. \tag{5}$$

In this way, the spectrum of the signal is the combination of the analog spectrum and digital spectrum. Taking the 33% RZ signal as an example, its spectrum is illustrated in Fig. 1(a), and the analog and digital spectra are illustrated in Figs. 1(b) and 1(c), respectively. It is clear that the envelop of the spectrum is determined by the analog spectrum, while the line spectral components and ripples of the spectrum are determined by the digital spectrum.

2.2 Analog spectrum

The analog part of the modulated signal is a pulse centered at $t = 0$, it can be either NRZ or RZ shape. The NRZ pulse is a gate function, which is expressed as

$$g(t) = \begin{cases} 1, & |t| \leqslant \frac{T_s}{2}, \\ 0, & |t| > \frac{T_s}{2}, \end{cases} \tag{6}$$

while the RZ pulse with duty cycle of 33% is described by [37]

$$g(t) = \begin{cases} \cos\left[\frac{\pi}{2}\sin\left(\frac{\pi}{T_s}t\right)\right], & |t| \leqslant \frac{T_s}{2}, \\ 0, & |t| > \frac{T_s}{2}. \end{cases} \tag{7}$$

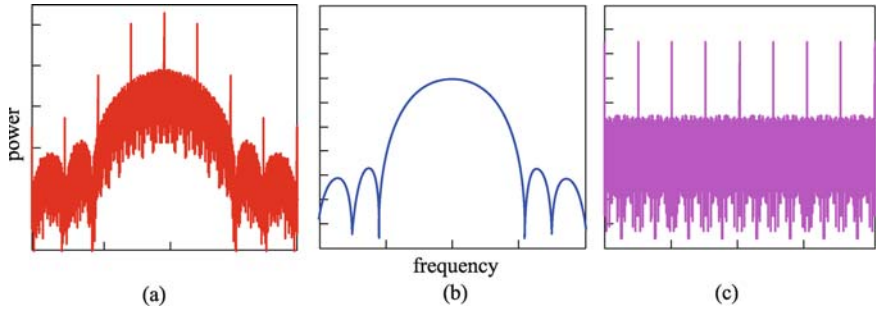

Fig. 1 (a) Spectrum, (b) analog spectrum and (c) digital spectrum of the 33% RZ signal

Figure 2(a) shows the NRZ and 33% RZ pulses with time duration of T_s. B is defined as the reciprocal of T_s, B = $1/T_s$, which denotes the baud rate of the signal. The analog spectrum of NRZ signal is shown in Fig. 2(b), it is Sinc-shaped. The bandwidths of the mainlobe and sidelobe are 2B and B, respectively. Whereas, on the other hand, the analog spectrum of RZ signal has an evidently larger mainlobe than that of NRZ signal.

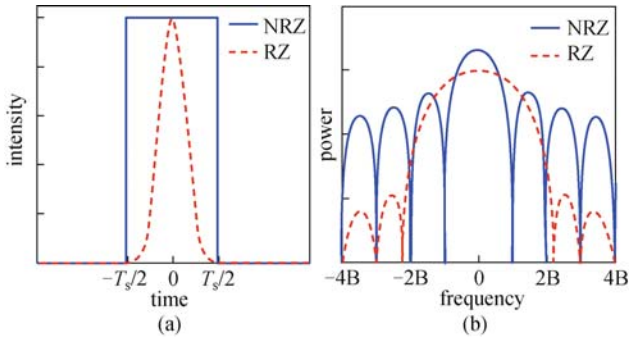

Fig. 2 (a) Analog part and (b) analog spectra of the NRZ and RZ signal

2.3 Digital spectrum

The digital spectrum is the Fourier transformation of the data information $\sum_{k=-\infty}^{+\infty} x_k\delta(t-kT_s)$, which is given by

$$F(f)=\int_{-\infty}^{+\infty}\sum_{k=-\infty}^{+\infty}x_k\delta(t-kT_s)\exp(-\mathrm{j}2\pi ft)\mathrm{d}t$$

$$=\sum_{k=-\infty}^{+\infty}x_k\exp(-\mathrm{j}2\pi f\cdot kT_s). \tag{8}$$

It can be seen that, $F(f)$ is periodic with period of B, which is exactly the baud rate of the signal. Thus the information of the symbol sequence is stored within a baud rate of the spectrum. In other words, the spectral components within each baud rate are enough to recover the total data information of the signals.

For the information symbol sequence with finite length of N, when transformed by the discrete Fourier transformation (DFT), there are N spectral components within a bandwidth of its baud rate, namely, B. It is noted that, the discrete spectral components within B tend to be continuous with increasing the symbol sequence length [38]. The information symbols of the signal are $\{x_0, x_1,\ldots, x_{N-1}\}$, and the complex amplitudes of the discrete spectral components within a baud rate are set as $\{X_1, X_2,\ldots, X_{N-1}\}$. The relationship between the information symbol sequence and the complex amplitude of the discrete spectral components are presented as

$$X_m=\frac{1}{N}\sum_{k=0}^{N-1}x_k\exp\left(-\mathrm{j}2\pi\frac{mk}{N}\right), \tag{9}$$

or

$$x_k=\sum_{m=0}^{N-1}X_m\exp\left(\mathrm{j}2\pi\frac{mk}{N}\right). \tag{10}$$

It can also be demonstrated via the matrix relationship.

$$\begin{bmatrix}X_0\\X_1\\\vdots\\X_{N-1}\end{bmatrix}=\frac{1}{N}\begin{bmatrix}1&1&\cdots&1\\1&\mathrm{e}^{-\mathrm{j}2\pi\frac{1}{N}}&\cdots&\mathrm{e}^{-\mathrm{j}2\pi\frac{N-1}{N}}\\\vdots&\vdots&\ddots&\vdots\\1&\mathrm{e}^{-\mathrm{j}2\pi\frac{N-1}{N}}&\cdots&\mathrm{e}^{-\mathrm{j}2\pi\frac{(N-1)(N-1)}{N}}\end{bmatrix}\cdot\begin{bmatrix}x_0\\x_1\\\vdots\\x_{N-1}\end{bmatrix}, \tag{11}$$

or

$$\begin{bmatrix}x_0\\x_1\\\vdots\\x_{N-1}\end{bmatrix}=\begin{bmatrix}1&1&\cdots&1\\1&\mathrm{e}^{\mathrm{j}2\pi\frac{1}{N}}&\cdots&\mathrm{e}^{\mathrm{j}2\pi\frac{N-1}{N}}\\\vdots&\vdots&\ddots&\vdots\\1&\mathrm{e}^{\mathrm{j}2\pi\frac{N-1}{N}}&\cdots&\mathrm{e}^{\mathrm{j}2\pi\frac{(N-1)(N-1)}{N}}\end{bmatrix}\cdot\begin{bmatrix}X_0\\X_1\\\vdots\\X_{N-1}\end{bmatrix}. \tag{12}$$

Taking OOK signal as an example, the information symbol sequence is Pseudo Random Binary Sequence (PRBS) with length of N. The digital spectrum is illustrated in Fig. 3. The spectral components are periodic. The discrete spectral components within B are $\{X_0, X_1, X_2,\ldots, X_{N-1}\}$, which are repeated by themselves. X_0 is the complex amplitude of zero frequency, it is also the line spectral component of the digital spectrum, that is

$$X_0 = \frac{1}{N}\sum_{k=0}^{N-1} x_k. \tag{13}$$

For the phase modulated signal, the x_k in the integration are cancelled by each other. Thus, there are no line spectral components in the spectra of phase modulated signal.

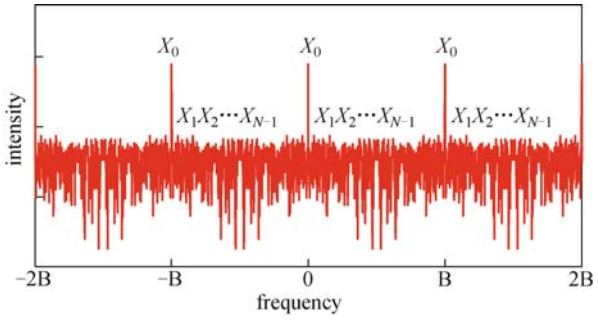

Fig. 3 Digital spectrum of the RZ signal

3 Operational principle for linear signal processing

3.1 Analog spectrum processing

In this section, the reported RZ-to-NRZ format conversion functions for intensity and phase modulated signals using DI [20–22,27,29,31–35] and MRRs [23–26,30] are theoretically analyzed and numerically simulated. Because the transmission spectrum of the through port of the MRR [39] is similar with the transmission spectrum of the DI, we take the DI as the filter to be analyzed. These format conversions could be illustrated with the analog spectrum conversion process. The pulse shape of each symbol is changed from RZ to NRZ, while the symbol sequence of the data information remains unchanged.

First, the RZ-pulse to NRZ-pulse conversion process is analyzed. Figure 4(a) shows a 33% RZ-pulse with duration time of T_s. Figure 4(b) shows the spectra of the RZ-pulse together with the transmission spectrum of the DI, which acts as a comb notch filter. The relative delay time of DI is $T_s/2$, so the free spectral range (FSR) is 2B. The transmission peak of the DI is aligned to the carrier frequency of the RZ-pulse. Figure 4(d) shows the spectrum of the converted NRZ-pulse in solid line. The mainlobe bandwidth of the converted NRZ pulse is 2B, which is

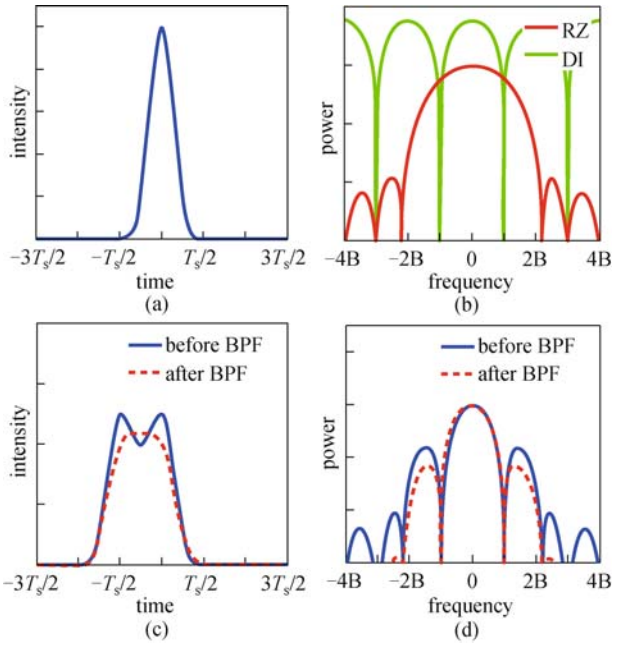

Fig. 4 (a) Waveform of the RZ pulse; (b) spectrum of the RZ pulse and the transmission spectrum of DI; (c) waveform and (d) spectrum of the converted NRZ pulse

exactly the mainlobe bandwidth of an ideal NRZ pulse with duration time of T_s (shown in Fig. 4(b)).

It should be mentioned that the sidelobe of the converted signal is not completely the same as that of an ideal NRZ pulse, which would induce intensity ripple at the top of the converted NRZ-pulse. Nevertheless, the intensity ripple of the top can be eliminated by a following band pass filter (BPF) (a Gaussian filter with 3 dB bandwidth of 2B). The waveforms and spectra of the converted NRZ-pulse processed before and after the BPF are illustrated in solid and dot line, as shown in Figs. 4(c) and 4(d), respectively. As a result, the conversion from 33% RZ-pulse to NRZ-pulse is realized by the DI.

The RZ signal is considered as an intermittent RZ pulse sequence. When transmitting through the DI, the spectrum of the converted signal is expressed as

$$F_{\text{out}}(f) = [G(f)\cdot H_{\text{DI}}(f)]\cdot X(f), \tag{14}$$

where $H_{\text{DI}}(f)$ is the transmission spectrum DI. $H_{\text{DI}}(f)$ can be expressed as

$$H_{\text{DI}}(f) = \frac{1}{2}[1+\cos(f\Delta T + \Delta\phi)],$$

where ΔT is the time delay and $\Delta\phi$ is the phase difference between two arms of the DI. The electric field of the converted signal is expressed as

$$E_{\text{out}}(t) = [g(t) * h_{\text{DI}}(t)] * \sum_{k=-\infty}^{+\infty} x_k\delta(t-kT_s), \tag{15}$$

where $h_{DI}(t)$ is the impulse response of the DI. Equation (15) indicated that the DI is supposed to solely operate on the analog part of the signal. As a result, the pulse shape of each symbol is changed from RZ to NRZ, while the information symbol sequence is unchanged. Figure 5 shows the operational principle for 33% RZ-OOK to NRZ-OOK format conversion using DI. The waveform of RZ signal is illustrated in Fig. 5(a). The symbol period of the RZ signal is T_s, and the baud rate is B. The spectra of the input RZ signal together with the transmission spectrum of the DI are illustrated in Fig. 5(b). The transmission peak of the DI is aligned to the carrier frequency of the RZ signal. The spectrum of the RZ signal is decomposed into the analog and digital spectra, as shown in Figs. 5(c) and 5(d), respectively. The DI solely operates on the analog spectrum of the RZ signal, which is converted to the analog spectrum of NRZ signal. The analog spectrum of the converted NRZ signal is illustrated in Fig. 5(g), whose mainlobe bandwidth is 2B. The spectrum of the converted NRZ signal, which consists of the converted NRZ analog spectrum (Fig. 5(g)) and the unchanged digital spectrum (Fig. 5(h)), is illustrated in Fig. 5(f). The waveform of the converted signal is illustrated in Fig. 5(e). It can be seen that the pulse shape of each symbol is changed from RZ to NRZ, while the information symbol sequence is unchanged.

Based on this operational principle, we have experimentally demonstrated format conversion functions from RZ to NRZ at 20 Gb/s [20], RZ with different duty cycles to NRZ at 20 Gb/s [21], CS-RZ to NRZ at 40 Gb/s [22] and RZ to NRZ at 40 Gb/s [23] with fiber-based DIs, RZ to NRZ at 640 Gb/s with SOI based MRR [26]. At the same time, thanks to the periodic nature of the DIs and MRRs, multichannel parallel format conversion have been demonstrated, such as 4 × 50 Gb/s RZ to NRZ conversion with MRR [24].

In addition to RZ-OOK signal, the RZ-DPSK and RZ-QPSK signal can also be converted to NRZ-DPSK and NRZ-QPSK signal using a DI. The numerical simulations are carried out under the same condition with RZ signal. The waveform of the converted NRZ-DPSK and NRZ-QPSK are illustrated in Figs. 6(a) and 6(b), respectively. The intensity ripple in the converted signal can be eliminated by a following BPF, which is similar to the case of RZ-OOK signal.

Similar with the NRZ-DPSK signal generated by a Mach-Zehnder modulator (MZM), the converted NRZ-DPSK signal has the intensity dips located at phase transitional points, due to the destructive interference between the adjacent converted NRZ pulses with phase difference of "π", as shown in Fig. 7. In this case, the intensity at the junction reduces to zero. Similarly, the converted QPSK has the same characteristic with the NRZ-QPSK signal generated by the nested MZMs, it has the intensity dips with different depths located at the phase transmission points, due to the destructive and incomplete interferences between the adjacent NRZ pulses with phase difference of "π" and "π/2" , respectively. The intensity at the junction with phase transition of "π" and "π/2" reduces to zero or to a certain degree, respectively.

The format conversion for RZ-DPSK to NRZ-DPSK and RZ-QPSK to NRZ-QPSK have been demonstrated experimentally [25,27,30,32,33]. Thanks to the polarization insensitivity and periodic nature of DI, the scheme is suitable for simultaneous PDM and WDM systems [31,34,35].

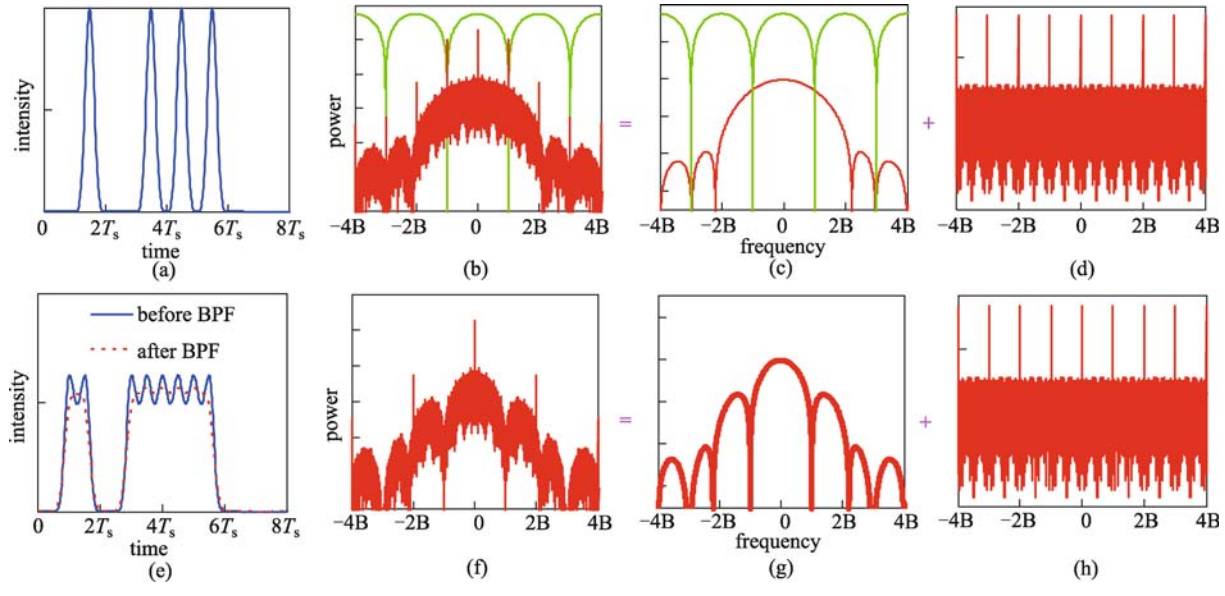

Fig. 5 (a) Waveform of the RZ signal; (b) spectrum of the RZ signal and the transmission spectrum of DI; (c) analog spectrum of the RZ signal and the transmission spectrum of DI; (d) digital spectrum of the RZ signal; (e) waveform, (f) spectrum, (g) analog spectrum, and (h) digital spectrum of the converted NRZ signal

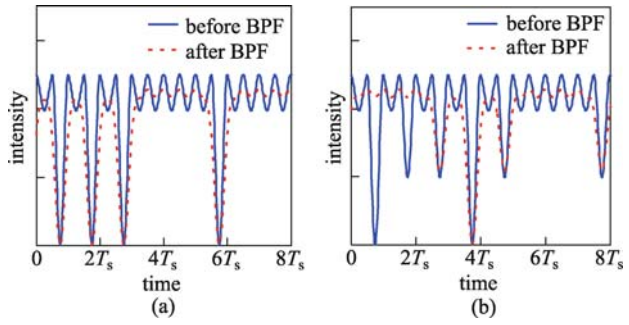

Fig. 6 Waveform of the converted (a) DPSK and (b) QPSK signals

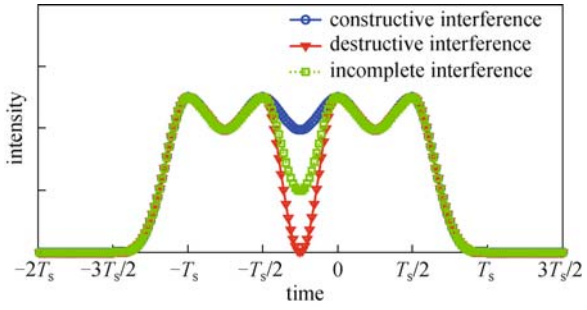

Fig. 7 Two adjacent converted NRZ pulses with different phase transitions

3.2 Digital spectrum processing

In this section, those reported linear signal processing functions such as all-optical logic NOT gate [13], clock recovery for RZ-OOK signal [14,36] and format conversions from (N)RZ-OOK to (N)RZ-PSK [40], and are theoretically analyzed and numerically simulated. These functions could be illustrated with digital spectrum conversion process. When transmitting through the filter, the spectrum of the converted signal is expressed as

$$F_{\text{out}}(f) = G(f) \cdot [X(f) \cdot H(f)], \tag{16}$$

where $H(f)$ is the transmission spectrum of the optical filter. The electric field of the converted signal is presented as

$$E_{\text{out}}(t) = g(t) * \left[\sum_{k=-\infty}^{+\infty} x_k \delta(t - kT_k) * h(t) \right], \tag{17}$$

where $h(t)$ is the impulse response of the filter, which is supposed to solely operates on the digital part of the signal. As a result, the information symbol sequence is converted from OOK to PSK, its logic NOT gate or clock, respectively, while the pulse shape of each symbol is remained.

For the RZ-OOK to RZ-PSK format conversion, the information symbol sequence {0, 1} are converted to {−1/2, 1/2}. Figure 8(a) shows the digital spectra of the OOK signal together with the transmission spectrum at

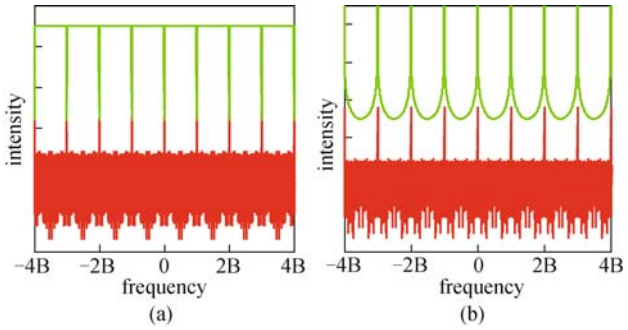

Fig. 8 Digital spectrum conversion for OOK to (a) PSK and (b) clock recovery

through port of the MRR, which acts as a comb notch filter [39]. The FSR of the MRR is equal to the period of the digital spectrum, and the resonance notches of the transmission spectrum of MRR aim at the line spectral components of the digital spectrum.

It should be mentioned that the requirement of the MRR for digital signal processing is totally different from that for analog signal processing. In this situation, one MRR with flat passband and sharp and deep notch should be exploited to realize the RZ-OOK to RZ-PSK format conversion. As a result, the zero-frequency X_0 of the digital spectrum is suppressed, while other frequency components remain unchanged. The information symbol "0" turns into "−1/2," while "1" turns into "1/2," which is deduced from the matrix expression below.

$$\begin{bmatrix} x_0 - \frac{1}{2} \\ x_1 - \frac{1}{2} \\ \vdots \\ x_{N-1} - \frac{1}{2} \end{bmatrix} = \begin{bmatrix} 1 & 1 & \cdots & 1 \\ 1 & e^{j2\pi\frac{1}{N}} & \cdots & e^{j2\pi\frac{N-1}{N}} \\ \vdots & \vdots & \ddots & \vdots \\ 1 & e^{j2\pi\frac{N-1}{N}} & \cdots & e^{j2\pi\frac{(N-1)(N-1)}{N}} \end{bmatrix} \cdot \begin{bmatrix} 0 \\ X_1 \\ \vdots \\ X_{N-1} \end{bmatrix}. \tag{18}$$

The operational principle for RZ-OOK to RZ-PSK format conversion is illustrated in Fig. 9. The waveform of RZ signal is illustrated in Fig. 9(a). The symbol period of the RZ signal is T_s, and the baud rate is B. The spectra of RZ signal together with the transmission spectrum of the through port of MRR are illustrated in Fig. 9(b). The FSR of the MRR is B, and the resonance notches of the MRR aim at the line spectral components of the RZ signal. The spectrum of the RZ signal is decomposed into the analog and digital spectra, as shown in Figs. 9(c) and 9(d), respectively. The MRR solely operates on the digital

spectrum of the RZ signal. The information symbol sequence of the RZ signal turns into the information symbol sequence of RZ-PSK signal. The spectrum of the converted RZ-PSK signal is illustrated in Fig. 9(f), which consists of the unchanged analog spectrum (Fig. 9(g)) and the converted RZ-PSK digital spectrum (Fig. 9(h)). The waveform of the converted RZ-PSK signal is illustrated in Fig. 9(e). The pulse shape of each symbol is unchanged.

The scheme is also suitable for the NRZ-OOK to NRZ-PSK format conversion, since the MRR only operates on the digital spectrum of the signal. The numerical simulations are carried out under the same condition with RZ signal, as illustrated in Fig. 10. The waveform and spectrum of the NRZ signal and the converted NRZ-PSK signal are illustrated in Figs. 10(a), (b), (c) and (d), respectively.

Considering the characteristic of the NRZ signal spectrum, the NRZ-OOK to NRZ-PSK format conversion can be actually realized by using a single band notch filter, since there is no line spectral components in the spectrum except for the carrier component, as can be seen from the spectrum of NRZ signal (illustrated in Fig. 10(b)). Thus, it is only necessary to suppress the carrier frequency component of the NRZ signal to achieve NRZ-OOK to NRZ-PSK format conversion. Similar with the MZM generated NRZ-PSK signal, the converted NRZ-PSK signal has the intensity dips located at phase transition points, due to the destructive interference between the adjacent converted NRZ pulses with phase difference of "π" .

While, for the clock recovery for RZ signal, the information symbol sequence {0, 1} turns into {1/2}. Figure 10(b) shows the digital spectra of the OOK signal together with the drop transmission spectrum of the MRR. The FSR of the MRR is equal to the baud rate of the RZ signal. Ideally, the resonance peaks of the drop transmission spectrum of MRR should be sharp and narrow enough to extract out only the line spectral components of the RZ-OOK signal. As a result, the zero-frequency X_0 of the digital spectrum is maintained while other spectral components are suppressed. The information symbols in the sequence all turn into "1/2", which is deduced from the matrix expression below.

$$\begin{bmatrix} 1/2 \\ 1/2 \\ \vdots \\ 1/2 \end{bmatrix} = \begin{bmatrix} 1 & 1 & \cdots & 1 \\ 1 & e^{j2\pi\frac{1}{N}} & \cdots & e^{j2\pi\frac{N-1}{N}} \\ \vdots & \vdots & \ddots & \vdots \\ 1 & e^{j2\pi\frac{N-1}{N}} & \cdots & e^{j2\pi\frac{(N-1)(N-1)}{N}} \end{bmatrix} \cdot \begin{bmatrix} X_0 \\ 0 \\ \vdots \\ 0 \end{bmatrix}. \tag{19}$$

The operational principle of the clock recovery for RZ-OOK signal is illustrated in Fig. 11. The waveform of the RZ signal is illustrated in Fig. 11(a). The symbol period of the RZ signal is T_s, and baud rate is B. The spectra of RZ signal together with the transmission spectrum of the drop port of MRR are illustrated in Fig. 11(b). The FSR of the MRR is B, and the resonance peaks of MRR are aligned to the line spectral components of the RZ signal. The

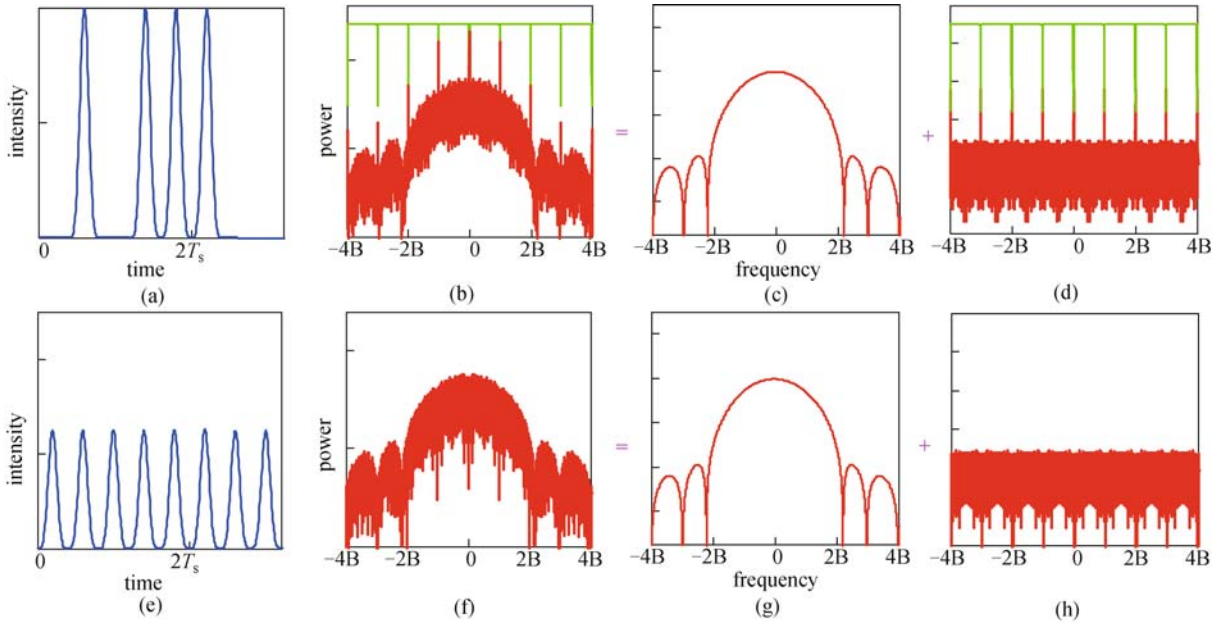

Fig. 9 (a) Waveform of the RZ signal; (b) spectrum of the RZ signal and the transmission spectrum of the through port of MRR; (c) analog spectrum of RZ signal; (d) digital spectrum of RZ signal and the transmission spectrum of MRR; (e) waveform, (f) spectrum, (g) analog spectrum, and (h) digital spectrum of the converted RZ-PSK signal

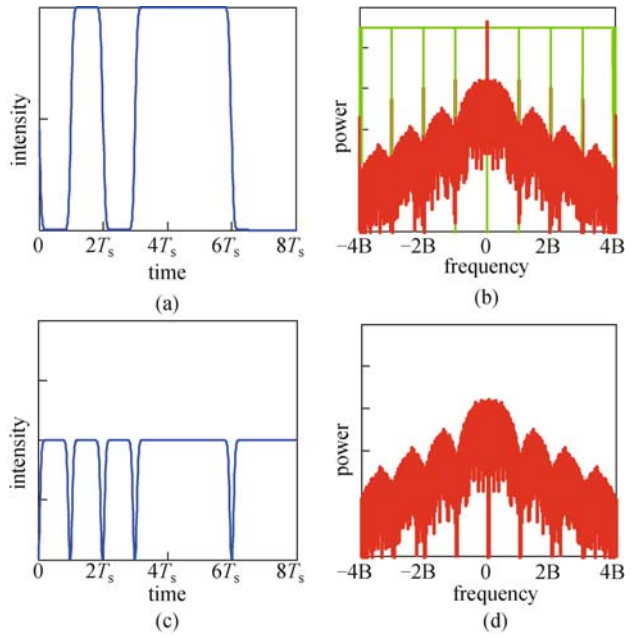

Fig. 10 (a) Waveform of the NRZ signal; (b) spectrum of the NRZ signal and the transmission spectrum of the through port of MRR; (c) waveform and (d) spectrum of the converted NRZ-PSK signal

spectrum of the RZ signal is decomposed into the analog and digital spectra, as shown in Figs. 11(c) and 11(d), respectively. The MRR solely operates on the digital spectrum of the RZ signal. The information symbol sequence of the RZ signal turns into the information symbol sequence of clock. The spectrum of the converted clock is illustrated in Fig. 11(f), which consists of the unchanged analog spectrum (Fig. 11(g)) and the converted clock digital spectrum (Fig. 11(h)). The waveform of the converted clock is illustrated in Fig. 11(e). The pulse shape of each symbol is unchanged.

For further investigation, Eqs. (18) and (19) can be combined together to realize other signal processing functions such as Eq. (19) − Eq. (18) denotes logic NOT gate [13], while Eq. (19) + jEq. (18) denotes clock recovery with phase-only filter [14], which are presented as below

$$\begin{bmatrix} 1-x_0 \\ 1-x_1 \\ \vdots \\ 1-x_{N-1} \end{bmatrix} = \begin{bmatrix} 1 & 1 & \cdots & 1 \\ 1 & e^{j2\pi\frac{1}{N}} & \cdots & e^{j2\pi\frac{N-1}{N}} \\ \vdots & \vdots & \ddots & \vdots \\ 1 & e^{j2\pi\frac{N-1}{N}} & \cdots & e^{j2\pi\frac{(N-1)(N-1)}{N}} \end{bmatrix} \cdot \begin{bmatrix} X_0 \\ -X_1 \\ \vdots \\ -X_{N-1} \end{bmatrix}, \tag{20}$$

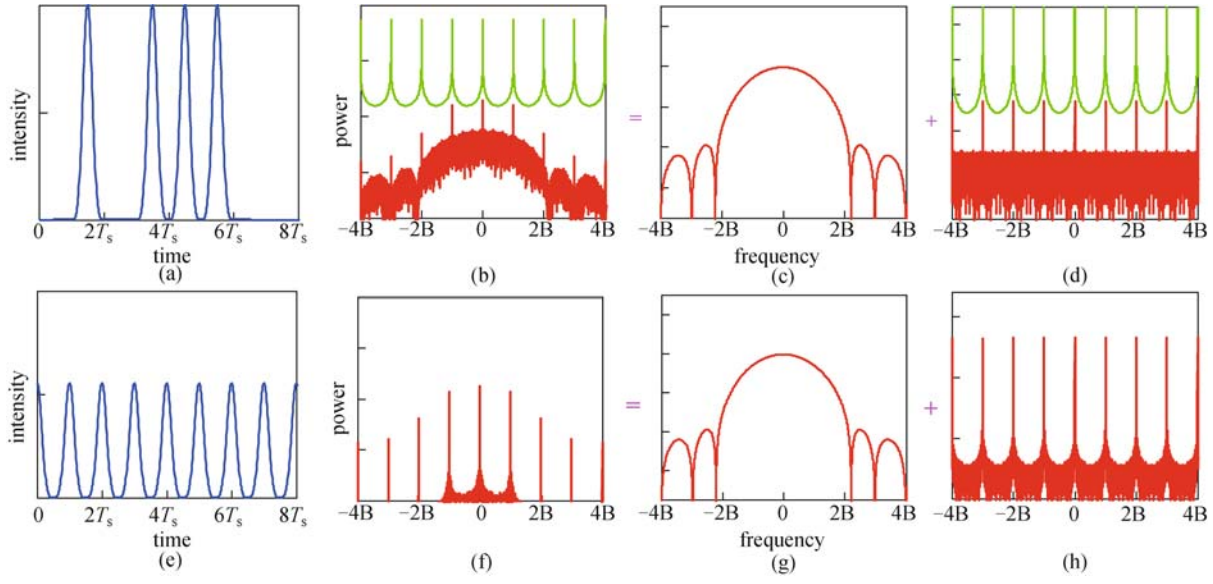

Fig. 11 (a) Waveform of the RZ signal; (b) spectrum of the RZ signal and the transmission spectrum of the drop port of MRR; (c) analog spectrum of the RZ signal; (d) digital spectrum of the RZ signal and the transmission spectrum of MRR; (e) waveform, (f) spectrum, (g) analog spectrum, and (h) digital spectrum of the recovered clock

$$\begin{bmatrix} \frac{1}{2}+j\left(x_0-\frac{1}{2}\right) \\ \frac{1}{2}+j\left(x_1-\frac{1}{2}\right) \\ \vdots \\ \frac{1}{2}+j\left(x_{N-1}-\frac{1}{2}\right) \end{bmatrix} = \begin{bmatrix} 1 & 1 & \cdots & 1 \\ 1 & e^{j2\pi\frac{1}{N}} & \cdots & e^{j2\pi\frac{N-1}{N}} \\ \vdots & \vdots & \ddots & \vdots \\ 1 & e^{j2\pi\frac{N-1}{N}} & \cdots & e^{j2\pi\frac{(N-1)(N-1)}{N}} \end{bmatrix} \cdot \begin{bmatrix} X_0 \\ jX_1 \\ \vdots \\ jX_{N-1} \end{bmatrix}. \quad (21)$$

For the logic NOT gate, the information symbol "0" turns into "1," while "1" turns into "0." In this case, the zero-frequency X_0 remains unchanged while other frequency components experience a phase shift of "π". On the other hand, for the clock recovery using phase-only filter, the information symbol "0" turns into "1/2 – 1/2j", while "1" turns into "1/2 + 1/2j". In this case, the zero-frequency X_0 remains unchanged while other frequency components experience a phase shift of "π/2".

4 Discussion

As discussed in Section 3, the presented method can be easily used to illustrate the operational principle of linear signal processing functions with filtering effect. Actually, the most important function of this method is providing the guidance of designing the optical filter. Usually, we cannot identify whether the optical filters operate on the analog spectrum or the digital spectrum, but we can optimize the optical filter according to the requirement of analog spectrum conversion or digital spectrum conversion. For analog spectrum conversion, we will alleviate its effect on the digital spectrum by optimizing the optical filter. Correspondingly, we should alleviate its effect on the analog spectrum for digital spectrum conversion. In this section, we will discuss the influence due to imperfectness of the optical filter and how to design the optical filter.

4.1 Designing method of the optical filter

For analog spectrum conversion, it is very easy to get the transmission spectrum of the optical filter according to the equation

$$H(f) = G_{\text{out}}(f)/G_{\text{in}}(f), \quad (22)$$

where $G_{\text{out}}(f)$ is the analog spectrum of the converted signal and $G_{\text{in}}(f)$ is the analog spectrum of the original input signal. It is very common in the textbook of signal and systems and there is nothing new for the optical signal.

For digital spectrum conversion, the situation is a little complicated. For an information symbols sequence of $x = \{x_0, x_1,..., x_{N-1}\}$ and its digital spectrum is $X = \{X_0, X_1,..., X_{N-1}\}$. According to Eqs. (11) and (12), with the Fourier transform matrix $\boldsymbol{F}$ and the inverse Fourier transform matrix $\boldsymbol{F}^{-1}$, we can get relations $\boldsymbol{X} = \boldsymbol{F}\boldsymbol{x}$ and $\boldsymbol{x} = \boldsymbol{F}^{-1}\boldsymbol{X}$, respectively.

If we want to transform the digital sequence $\boldsymbol{x} = \{x_0, x_1,..., x_{N-1}\}$ to a new digital sequence $\boldsymbol{y} = \{y_0, y_1,..., y_{N-1}\}$ via the optical filter, the transforming operation can be expressed by a matrix $\boldsymbol{M}$,

$$\boldsymbol{y} = \boldsymbol{M}\boldsymbol{x}. \quad (23)$$

Then, we can get the transmission spectrum of the optical filter through the following expression,

$$\boldsymbol{H} = \boldsymbol{F}\boldsymbol{M}\boldsymbol{F}^{-1}, \quad (24)$$

and

$$\boldsymbol{M} = \boldsymbol{F}^{-1}\boldsymbol{H}\boldsymbol{F}. \quad (25)$$

Theoretically, for arbitrary matrix $\boldsymbol{M}$, we can get a corresponding optical filter to realize this transforming process. However, some filters are very difficult to be realized physically. When the transmission matrix is a diagonal matrix, the situation is the simplest, and it is the easiest to fabricate this kind of optical filter. In some case, even the matrix is not a diagonal matrix, but when the diagonal components are dominant comparing with other components, we can use the diagonal matrix only with those diagonal components to represent the transforming matrix. For this situation, the transforming matrix is

$$\boldsymbol{H} = \text{diag}\{\boldsymbol{F}\boldsymbol{M}\boldsymbol{F}^{-1}\}, \quad (26)$$

where

$$\boldsymbol{H}_k = [\boldsymbol{F}\boldsymbol{M}\boldsymbol{F}^{-1}]_{(k,k)}, \quad k = 0,1,...,N-1. \quad (27)$$

For the above discussed digital signal processing functions, NRZ-OOK to NRZ-PSK conversion, all-optical clock recovery and all-optical logic NOT gate could be realized with the following three ideal transforming matrixes:

$$\boldsymbol{H}_{\text{OOK-PSK}} = \begin{bmatrix} 0 & 0 & \cdots & 0 \\ 0 & 1 & \cdots & 0 \\ \vdots & \vdots & \ddots & \vdots \\ 0 & 0 & \cdots & 1 \end{bmatrix}, \quad (28)$$

$$\boldsymbol{H}_{\text{clock recovery}} = \begin{bmatrix} 1 & 0 & \cdots & 0 \\ 0 & 0 & \cdots & 0 \\ \vdots & \vdots & \ddots & \vdots \\ 0 & 0 & \cdots & 0 \end{bmatrix} \text{ or } \begin{bmatrix} 1 & 0 & \cdots & 0 \\ 0 & j & \cdots & 0 \\ \vdots & \vdots & \ddots & \vdots \\ 0 & 0 & \cdots & j \end{bmatrix}, \quad (29)$$

$$\boldsymbol{H}_{\mathrm{NOT-gate}}=\begin{bmatrix}1 & 0 & \cdots & 0\\ 0 & -1 & \cdots & 0\\ \vdots & \vdots & \ddots & \vdots\\ 0 & 0 & \cdots & -1\end{bmatrix}. \tag{30}$$

In these cases of digital signal processing, the transmission spectrum of the filter is periodic with period equal to the baud rate of the signal. Whereas, if the period of the spectrum is the integer times of the baud rate [39], this signal conversion can also be analyzed by the digital signal processing. In Ref. [39], the information symbols sequence $\boldsymbol{x}=\{x_0, x_1,..., x_{N-1}\}$ is regarded as $\{x_0,0,x_1,0,...,x_{N-1},0\}$ and its digital spectrum is $\{X_0, X_1,..., X_{N-1},X_0, X_1,..., X_{N-1}\}$, since the period of the filter's transmission spectrum is two times of the signal's baud rate. After the filter, the digital spectrum is converted to $\{X_0, X_1,..., X_{N-1},-X_0, X_1,..., X_{N-1}\}$, and the information symbol is converted to $\left\{x_0-\frac{1}{2},\frac{1}{2},x_1-\frac{1}{2},\frac{1}{2},...,x_{N-1}-\frac{1}{2},\frac{1}{2}\right\}$. As a result, the waveform of the RZ signal is converted to the NRZ waveform.

4.2 Error analysis due to imperfectness of the optical filter

Usually, there exist some deviations between actual filter and ideal filter which will induce additional errors into the converted output signals. Taking the (N)RZ to (N)RZ-PSK conversion as example, if the resonance notch of the MRR is not sharp or deep enough, the zero frequency component is not suppressed to zero, and other spectral components $\{X_1, X_2,..., X_{N-1}\}$ are also changed identically in each period. In this case, the recovered information symbol sequence is changed according to the matrix relationship.

$$\begin{bmatrix}y_0\\ y_1\\ \vdots\\ y_{N-1}\end{bmatrix}=\begin{bmatrix}1 & 1 & \cdots & 1\\ 1 & \mathrm{e}^{\mathrm{j}2\pi\frac{1}{N}} & \cdots & \mathrm{e}^{\mathrm{j}2\pi\frac{N-1}{N}}\\ \vdots & \vdots & \ddots & \vdots\\ 1 & \mathrm{e}^{\mathrm{j}2\pi\frac{N-1}{N}} & \cdots & \mathrm{e}^{\mathrm{j}2\pi\frac{(N-1)(N-1)}{N}}\end{bmatrix}\cdot\begin{bmatrix}X_0H_0\\ X_1H_1\\ \vdots\\ X_{N-1}H_{N-1}\end{bmatrix}. \tag{31}$$

Comparing with ideal filtering processing, imperfect MRR will introduce additional amplitude fluctuations into the converted output signal. That will induce OSNR reduction. Results show that there is no additional phase noise in this OOK to PSK conversion process. The following analysis can demonstrate this point.

For the OOK signal, the information symbol $\{x_0, x_1,..., x_{N-1}\}$ are real numbers. The complex amplitude of the digital spectrum components in a baud rate are conjugate-symmetric, as derived below.

$$\begin{aligned}X_{N-m}&=\frac{1}{N}\sum_{k=0}^{N-1}x_k\exp\left[-\mathrm{j}2\pi\frac{(N-m)k}{N}\right]\\ &=\frac{1}{N}\sum_{k=0}^{N-1}x_k\exp\left(\mathrm{j}2\pi\frac{mk}{N}\right)\\ &=\left\{\frac{1}{N}\sum_{k=0}^{N-1}x_k\exp\left(-\mathrm{j}2\pi\frac{mk}{N}\right)\right\}^*\\ &=X_m^*.\end{aligned} \tag{32}$$

The transmission spectrum of the MRR is conjugate-symmetric as well [41].

$$H_m=H_{N-m}^*. \tag{33}$$

The converted information symbol is deduced according to the inverse DFT as below.

$$\begin{aligned}y_k&=\sum_{m=0}^{N-1}X_mH_m\exp\left(\mathrm{j}2\pi\frac{mk}{N}\right)\\ &=X_0H_0+\sum_{m=1}^{[N/2]}\left[X_mH_m\exp\left(\mathrm{j}2\pi\frac{mk}{N}\right)\right.\\ &\quad\left.+X_{N-m}H_{N-m}\exp\left(\mathrm{j}2\pi\frac{(N-m)k}{N}\right)\right],\end{aligned} \tag{34}$$

where

$$\begin{aligned}&X_{N-m}H_{N-m}\exp\left(\mathrm{j}2\pi\frac{(N-m)k}{N}\right)\\ &=\left[X_mH_m\exp\left(\mathrm{j}2\pi\frac{mk}{N}\right)\right]^*.\end{aligned} \tag{35}$$

So that

$$\begin{aligned}y_k&=\sum_{m=0}^{N-1}X_mH_m\exp\left(\mathrm{j}2\pi\frac{mk}{N}\right)\\ &=X_0H_0+2\sum_{m=1}^{[N/2]}\mathrm{Re}\left\{X_mH_m\exp\left(\mathrm{j}2\pi\frac{mk}{N}\right)\right\},\end{aligned} \tag{36}$$

where $Re\{\cdot\}$ denotes the real part of $\cdot$. The information symbols are real number. That is to say, there is no phase noise induced by the imperfect MRR.

The simulated result of RZ-OOK to RZ-PSK format conversion and clock recovery for RZ-OOK using imperfect MRRs are illustrated in Figs. 12 and 13, respectively.

The spectra of the RZ signal together with the transmission spectra at the through port and drop port of MRR are illustrated in Figs. 12(a) and 13(a), respectively. The constellations of the converted RZ-PSK signal and the

recovered clock are illustrated in Figs. 12(b) and 13(b), respectively. It can be seen that there is only amplitude noise but no phase noise on the generated signal.

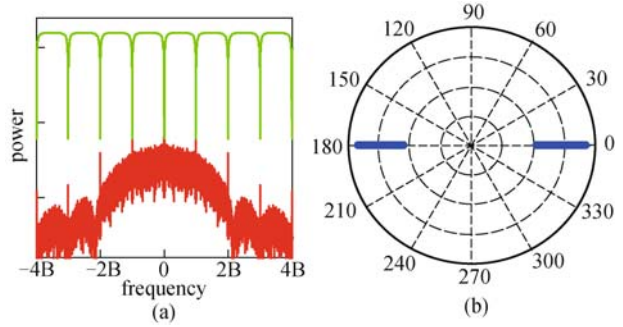

Fig. 12 (a) Spectrum of the 33% RZ signal and the through transmission spectrum of imperfect MRR; (b) constellation diagram of the converted RZ-PSK signal

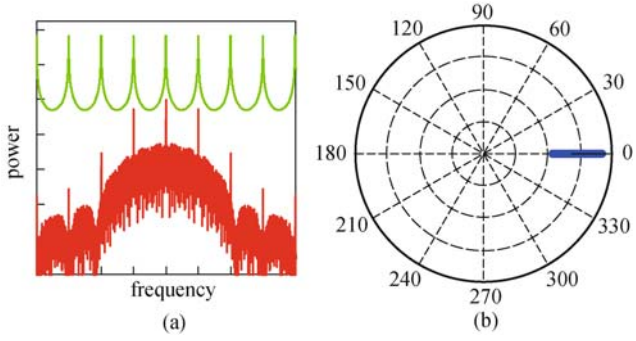

Fig. 13 (a) Spectrum of the 33% RZ signal and the drop transmission spectrum of imperfect MRR; (b) constellation diagram of the recovered clock

5 Conclusions

In this paper, an effective theoretical analysis method was presented to illustrate the experimental works of our group and other groups for all-optical linear signal processing with optical filters. The optical spectrum of the optical signal was decomposed into analog spectrum and digital spectrum, and the filters were supposed to operate individually on the analog part or the digital part of the signal for different applications. Those reported RZ to NRZ format conversions for OOK, DPSK, QPSK, multi-channel, PDM signals are based on analog spectrum conversion process, while those reported schemes for OOK to PSK format conversion, logic NOT gate and clock recovery for RZ signal are based on digital spectrum conversion process. The proposed method is very helpful for optimizing the optical filters for different applications. The designing method of the optical filter for analog spectrum conversion and digital spectrum conversion is discussed, and the transmission matrix can be easily used to design the optical filter for digital spectrum conversion. Error analysis due to imperfect filtering process was also discussed. Results show that the defective MRR for the digital spectrum conversion introduces only amplitude noise on the converted signal. The theoretical analysis proved that the optical filter has the potential to be used to realize arbitrary linear signal processing functions if only we could get corresponding optical filters.

Acknowledgements The authors would like to thank Prof. José Azaña from INRS in Canada for helpful suggestions in preparing the manuscript. This work was supported in part by the National Basic Research Program of China (No. 2011CB301704), the Nature Science Fund for Distinguished Young Scholars (No. 61125501), the National Natural Science Foundation of China (NSFC) Major International Joint Research Project (Grant No. 61320106016) and Foundation for Innovative Research Groups of the Natural Science Foundation of Hubei Province (No. 2014CFA004).

References

1. Ta'eed V G, Fu L, Pelusi M, Rochette M, Littler I C, Moss D J, Eggleton B J. Error free all optical wavelength conversion in highly nonlinear As-Se chalcogenide glass fiber. Optics Express, 2006, 14 (22): 10371–10376
2. Ta'eed V G, Shokooh-Saremi M, Fu L, Littler I C M, Moss D J, Rochette M, Eggleton B J, Yinlan Ruan B, Luther-DaviesB. Self-phase modulation-based integrated optical regeneration in chalcogenide waveguides. IEEE Journal of Selected Topics in Quantum Electronics, 2006, 12(3): 360–370
3. Bogoni A, Wu X, Nuccio S R, Willner A E. 640 Gb/s all-optical regenerator based on a periodically poled lithium niobate waveguide. Journal of Lightwave Technology, 2012, 30(12): 1829–1834
4. Yu Y, Zhang X, Rosas-Fernández J B, Huang D, Penty R V, White I H. Single SOA based 16 DWDM channels all-optical NRZ-to-RZ format conversions with different duty cycles. Optics Express, 2008, 16(20): 16166–16171
5. Chen X B, Yu Y, Zhang X L. All-optical logic minterms for three-input demodulated differential phase-shift keying signals at 40 Gb/s. IEEE Photonics Technology Letters, 2011, 23(2): 118–120
6. Wang F, Yu Y, Zhang Y, Zhang X. All-optical clock recovery using a single Fabry-Perot semiconductor optical amplifier. Journal of Lightwave Technology, 2012, 30(11): 1632–1637
7. Luo T, Yu C, Pan Z, Wang Y, McGeehan J E, Adler M, Willner A E. All-optical chromatic dispersion monitoring of a 40-Gb/s RZ signal by measuring the XPM-generated optical tone power in a highly nonlinear fiber. IEEE Photonics Technology Letters, 2006, 18(2): 430–432
8. Li J, Olsson B E, Karlsson M, Andrekson P A. OTDM add-drop multiplexer based on XPM-induced wavelength shifting in highly nonlinear fiber. Journal of Lightwave Technology, 2005, 23(9): 2654–2661
9. Fok M P, Shu C. Multipump four-wave mixing in a photonic crystal fiber for 6 times 10 Gb/s wavelength multicasting of DPSK signals. IEEE Photonics Technology Letters, 2007, 19(15): 1166–1168
10. Ye T, Yan C, Lu Y, Liu F, Su Y. All-optical regenerative NRZ-to-RZ format conversion using coupled ring-resonator optical waveguide. Optics Express, 2008, 16(20): 15325–15331
11. Lyubomirsky I, Chien C C, Wang Y H. Optical DQPSK receiver

with enhanced dispersion tolerance. IEEE Photonics Technology Letters, 2008, 20(7): 511–513
12. Zhang L, Yang J Y, Li Y, Song M, Beausoleil R G, Willner A E. Monolithic modulator and demodulator of differential quadrature phase-shift keying signals based on silicon microrings. Optics Letters, 2008, 33(13): 1428–1430
13. Maram R, Ming L, Azana J. High-speed all-optical NOT gate based on spectral phase-only linear optical filtering. In: Proceedings of IEEE Optical Fiber Communication Conference and Exposition and the National Fiber Optic Engineers Conference (OFC/NFOEC), 2013, 1–3
14. Maram R, Kong D, Galili M, Oxenløwe L K, Azaña J. Ultrafast all-optical clock recovery based on phase-only linear optical filtering. Optics Letters, 2014, 39(9): 2815–2818
15. Ashrafi R, Azaña J. Figure of merit for photonic differentiators. Optics Express, 2012, 20(3): 2626–2639
16. Ferrera M, Park Y, Razzari L, Little B E, Chu S, Morandotti R, Moss JD J, Azaña. Ultra-fast integrated all-optical integrator. In: Proceedings of Conference on Lasers and Electro-Optics (CLEO) and Quantum Electronics and Laser Science Conference (QELS), 2010, 1–2
17. Ferrera M, Park Y, Razzari L, Little B E, Chu S T, Morandotti R, Moss D J, Azaña J. All-optical 1st and 2nd order integration on a chip. Optics Express, 2011, 19(23): 23153–23161
18. Ngo N Q, Song Y. On the interrelations between an optical differentiator and an optical Hilbert transformer. Optics Letters, 2011, 36(6): 915–917
19. Asghari M H, Azaña J. All-optical Hilbert transformer based on a single phase-shifted fiber Bragg grating: design and analysis. Optics Letters, 2009, 34(3): 334–336
20. Yu Y, Zhang X L, Huang D X. All-optical RZ-to-NRZ format conversion with a tunable fibre based delay interferometer. Chinese Physics Letters, 2007, 24(3): 706–709
21. Yu Y, Zhang X L, Huang D X, Li L J, Fu W. 20-Gb/s all-optical format conversions from RZ signals with different duty cycles to NRZ signals. IEEE Photonics Technology Letters, 2007, 19(14): 1027–1029
22. Yu Y, Zhang X, Huang D. All-optical format conversion from CS-RZ to NRZ at 40 Gbit/s. Optics Express, 2007, 15(9): 5693–5698
23. Zhang Y, Xu E, Huang D, Zhang X. All-optical format conversion from RZ to NRZ utilizing microfiber resonator. IEEE Photonics Technology Letters, 2009, 21(17): 1202–1204
24. Ding Y, Peucheret C, Pu M, Zsigri B, Seoane J, Liu L, Xu J, Ou H, Zhang X, Huang D. Multi-channel WDM RZ-to-NRZ format conversion at 50 Gbit/s based on single silicon microring resonator. Optics Express, 2010, 18(20): 21121–21130
25. Ding Y, Xu J, Peucheret C, Pu M, Liu L, Seoane J, Ou H, Zhang X, Huang D. Multi-channel 40 Gbit/s NRZ-DPSK demodulation using a single silicon microring resonator. Journal of Lightwave Technology, 2011, 29(5): 677–684
26. Ding Y, Hu H, Galili M, Xu J, Liu L, Pu M, Mulvad H C, Oxenløwe L K, Peucheret C, Jeppesen P, Zhang X, Huang D, Ou H. Generation of a 640 Gbit/s NRZ OTDM signal using a silicon microring resonator. Optics Express, 2011, 19(7): 6471–6477
27. Zhang Z, Yu Y, Zhang X. Simultaneous all-optical demodulation and format conversion for multi-channel (CS)RZ-DPSK signals. Optics Express, 2011, 19(13): 12427–12433
28. Xiong M, Ding Y, Zhang Q, Zhang X. All-optical clock recovery from 40 Gbit/s RZ signal based on microring resonators. Applied Optics, 2011, 50(28): 5390–5396
29. Yu Y, Zhang X L, Huang D X. Simultaneous all-optical multi-channel RZ and CSRZ to NRZ format conversion. Optics Communications, 2011, 284(1): 129–135
30. Xiong M, Ozolins O, Ding Y, Huang B, An Y, Ou H, Peucheret C, Zhang X. Simultaneous RZ-OOK to NRZ-OOK and RZ-DPSK to NRZ-DPSK format conversion in a silicon microring resonator. Optics Express, 2012, 20(25): 27263–27272
31. Wu W, Yu Y, Hu S, Zou B, Zhang X. All-optical format conversion for polarization and wavelength division multiplexed system. IEEE Photonics Technology Letters, 2012, 24(18): 1606–1609
32. Zou B, Yu Y, Huang X, Wu Z, Wu W, Zhang X. All-optical format conversion for multichannel QPSK signals. Journal of Lightwave Technology, 2013, 31(3): 375–384
33. Xiang L, Gao D, Zou B, Hu S, Zhang X. Simultaneous multi-channel RZ-OOK/DPSK to NRZ-OOK/DPSK format conversion based on integrated delay interferometers and arrayed-waveguide grating. Science China-Technological Sciences, 2013, 56(3): 558–562
34. Qin Y, Yu Y, Zou J, Ye M, Xiang L, Zhang X. Silicon based polarization insensitive filter for WDM-PDM signal processing. Optics Express, 2013, 21(22): 25727–25733
35. Xiang L, Yu Y, Qin Y, Zou J, Zou B, Zhang X. SOI based ultracompact polarization insensitive filter for PDM signal processing. Optics Letters, 2013, 38(14): 2379–2381
36. Zou J, Yu Y, Yang W, Wu Z, Ye M, Chen G, Liu L, Deng S, Zhang X. An SOI based polarization insensitive filter for all-optical clock recovery. Optics Express, 2014, 22(6): 6647–6652
37. Winzer P J, Essiambre R J. Advanced optical modulation formats. Proceedings of the IEEE, 2006, 94(5): 952–985
38. Vaseghi S V. Advanced Signal Processing and Digital Noise Reduction. New York: Wiley, 1996
39. Maram R, Kong D, Galili M, Oxenlowe L K, Azana J. 640 Gbit/s RZ-to-NRZ format conversion based on optical phase filtering. In: Proceedings of IEEE Photonics Conference (IPC), 2014, 316–317
40. Ye T, Lu Y, Liu F, Zhang Q, Zhang Z, Qiu M, Su Y. 160-Gb/s NRZ-to-PSK conversion using linear filtering in silicon ring resonators. In: Proceedings of Lasers and Electro-Optics 2008 and 2008 Conference on Quantum Electronics and Laser Science (CLEO/QELS), 2008, JWA94
41. Heebner J, Grover R, Ibrahim T. Optical Microresonators: Theory, Fabrication, and Applications. Berlin: Springer, 2007

Prof. Xinliang Zhang received the B.S. and Ph.D. degrees from Huazhong University of Science and Technology (HUST), China, in 1992 and 2001. He became a full professor of HUST in 2004. Currently, he is the dean of the school of optical and electronic information, and the deputy director of the Wuhan National Laboratory for Optoelectronics. His research areas cover semiconductor optoelectronic

devices for optical interconnection and optical signal processing. He has over 300 publications in prestigious international journals and conferences, including over 160 IEEE Letters/Journals, *Optics Letters* or *Optics Express* and 30 OFC/ECOC papers. He holds 10 Chinese patents and 1 US patent. He is a senior member of IEEE and also a member of OSA.